Gas flows through constricted shallow micro-channels

A. GAT, I. FRANKEL AND D. WEIHS

Faculty of Aerospace Engineering, Technion - Israel Institute of Technology, Haifa 32000, Israel

We study the viscous compressible flow through micro-channels of non-uniform cross-section. A lubrication approximation is applied to analyse the flow through shallow configurations whose gap width is small in comparison with the other characteristic dimensions. Focusing on channels with a symmetric constriction (or cavity) we obtain the solution to the problem by means of a Schwarz–Christoffel transformation. This analytic solution is verified by examining the convergence of numerical simulations with diminishing Reynolds number and gap width. Explicit closed-form expressions for the pressure-head and mass-flow-rate losses in terms of the geometrical parameters characterizing the constriction are presented and discussed in the context of experimental data existing in the literature.

1. Introduction

With the advent of micro-fabrication technology micro-fluidics has become relevant to a rapidly growing spectrum of applications. Many of these applications (e.g. flow control, cooling in micro-electronic systems, etc.) involve gas flows through micro-configurations (Ho & Tai 1996, 1998; Gad-el-Hak 1999). Most of the research in micro-fluidic systems has so far focused on straight and uniform channels which constitute the simplest geometrical configuration while representing a basic element in practically all applications. Typically, the longitudinal and transverse dimensions of these channels are $\approx 10^3 - 10^4$ μm and $10 - 10^2$ μm, respectively. Pressure-driven flows are therefore dominated by high viscous resistance. Substantial density variations appear as the result of the large pressure drop involved which, however, are only accompanied by relatively minor accelerations. A clear indication of this 'low-Mach-number compressibility' is a nonlinear streamwise pressure variation as observed in the experiments of Pong, Ho & Tai (1994) and Liu, Tai & Ho (1995). Such non-uniform longitudinal pressure gradients were obtained in one-dimensional analyses of compressible viscous flows at small Reynolds and Mach numbers through circular cylindrical tubes (Prud'homme, Chapman & Bowen 1986; Berg, Seldam & Gulik 1993). Following these analyses and neglecting transverse velocity and pressure gradient, Harley *et al.* (1995) obtained an approximate solution for a one-dimensional channel flow. All of the above analyses neglect rarefaction effects. They are thus strictly valid only when Kn, the Knudsen number representing the ratio between the molecular mean free path and the macroscopic length scale, is vanishingly small. (Practically, the continuum hypothesis applies for $Kn \lesssim 10^{-3}$, cf. Cercignani 2000). However, for micro-channels at standard atmospheric conditions $Kn \approx 10^{-1} - 10^{-2}$. In this slip-flow domain the standard continuum model needs to be modified through the incorporation of velocity-slip and temperature-jump conditions at the channel

walls. This correction has been applied to micro-channel flows in a series of papers by Beskok and Karniadakis (Beskok, Karniadakis & Trimmer 1996, and references cited therein).

Micro-channel configurations are often shallow in the sense that the flow essentially takes place within the narrow ($\approx 1\,\mu\text{m}$) gap between parallel plates (cf. Harley *et al.* 1995; Arkilic, Schmidt & Breuer 1997; Zohar *et al.* 2002). Arkilic *et al.* (1997) have accordingly applied a lubrication approximation to obtain closed-form expressions for the mass-flow-rate and pressure distribution in a low-Mach-number compressible viscous slip flow in a straight and uniform channel. Their analytic and experimentally results have since been validated independently (e.g. Fan, Xue & Shu 1999; Zohar *et al.* 2002; Graur, Meolans & Zeitoun 2005, as well as others) and are widely referred to in the literature concerning gaseous micro-flows (Sharipov 1999; Yao *et al.* 2004; Qin, Sun & Yin 2007, as well as others).

It is important to note that complex geometries including such elements as channel junctions and branches, sudden expansions and contractions, etc. are of considerable relevance in micro-fluidics (e.g. channel networks, fuel cell devices, etc. Lee, Wong & Zohar 2001, 2002*a*; Tsai *et al.* 2007). However, in the absence of more suitable analyses, Arkilic *et al.*'s analysis is still used to correlate and interpret results pertaining to flows through essentially non-uniform channels (Lee *et al.* 2001, 2002*b*; Yu *et al.* 2005). The thrust of our contribution is therefore the extension of existing analyses of compressible viscous flows to configurations of non-uniform cross-section.

The rest of this paper is organized as follows: In the next section we formulate the general dimensionless problem governing the flow in shallow channels within the framework of the lubrication approximation. In §3 the problem is transformed to a Neumann problem for an appropriately defined quadratic function of the pressure, which is subsequently solved for a symmetric constriction or cavity by means of a Schwarz–Christoffel transformation. Explicit results for the pressure and mass-flow-rate losses are presented and discussed in §4 in terms of the geometrical parameters characterizing the constriction. The asymptotic calculations leading to these results are outlined in the Appendix.

2. Formulation of the problem

The steady motion of a perfect gas is governed by the continuity equation

$$\tilde{\nabla} \cdot (\tilde{\rho}\tilde{\boldsymbol{u}}) = 0, \tag{2.1}$$

the equation of motion (neglecting the effects of gravity)

$$\tilde{\rho}\tilde{\boldsymbol{u}} \cdot \tilde{\nabla}\tilde{\boldsymbol{u}} = -\tilde{\nabla}\tilde{p} + \tilde{\nabla} \cdot \tilde{\boldsymbol{\tau}}, \tag{2.2}$$

the energy equation

$$\tilde{\rho}C_v\tilde{\boldsymbol{u}} \cdot \tilde{\nabla}\tilde{T} = -\tilde{\nabla} \cdot \tilde{\boldsymbol{q}} - \tilde{p}\tilde{\nabla} \cdot \tilde{\boldsymbol{u}} + \tilde{\boldsymbol{\tau}} : \tilde{\nabla}\tilde{\boldsymbol{u}} \tag{2.3}$$

and the equation of state.

$$\tilde{p} = \tilde{\rho}R\tilde{T}. \tag{2.4}$$

In (2.1)–(2.4), $\tilde{\boldsymbol{u}}$ is the velocity vector and $\tilde{\rho}$, $\tilde{T}$ and $\tilde{p}$ denote the fluid density, temperature and pressure, respectively, R is the gas constant and C_v is the specific heat capacity at constant volume. For a Newtonian fluid the stress tensor is

$$\tilde{\boldsymbol{\tau}} = \mu\left(\tilde{\nabla}\tilde{\boldsymbol{u}} + \tilde{\nabla}\tilde{\boldsymbol{u}}^t\right) - \left(\tfrac{2}{3}\mu - \lambda\right)(\tilde{\nabla} \cdot \tilde{\boldsymbol{u}})\boldsymbol{I}, \tag{2.5}$$
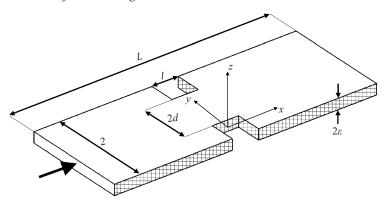
FIGURE 1. A schematic view of the constricted micro-channel defining the geometrical parameters l, d and L and the coordinate axes. (All dimensions are scaled by D, half the channel width.)

wherein μ and λ are, respectively, the shear and bulk viscosity coefficients. The heat flux-density vector is given by Fourier's equation

$$\tilde{\boldsymbol{q}} = -k\tilde{\nabla}\tilde{T}, \tag{2.6}$$

where k is the heat conductivity. We employ a Cartesian coordinate system $(\tilde{x}, \tilde{y}, \tilde{z})$ where the $\tilde{x}$- and $\tilde{y}$-axes are in the longitudinal and lateral directions, respectively, in the mid-plane of the channel and $\tilde{z}$ is perpendicular thereto (see figure 1). The x, y dimensionless coordinates (tildes are omitted in the notation of dimensionless variables) are normalized by D, the half-width of the uniform segments upstream and downstream of the constriction, while z is scaled by H, half the channel depth. Subsequent analysis focuses on a shallow micro-channel where

$$\varepsilon = \frac{H}{D} \ll 1. \tag{2.7}$$

For long shallow micro-channels with uninsulated walls maintained at uniform temperature, we follow the common practice in assuming an isothermal flow (see Arkilic *et al.* 1997; Harley *et al.* 1995, and the conclusion of this section). In this case μ, λ and k are uniform throughout the fluid. We normalize the pressure by an appropriate reference value p_0 of the pressure drop. The x and y components of $\boldsymbol{u}$, u and v respectively, are normalized by $U = p_0 H^2/\mu D$ reflecting the dominant balance in the equation of motion (2.2) between the pressure gradient and the viscosity terms (the inertial effects being negligible; cf. Graur *et al.* 2005). The corresponding z component, w, is accordingly scaled by εU. The reference density is selected in accordance with (2.4), to obtain its dimensionless counterpart as in (2.12). When $\varepsilon \to 0$ the leading order obtained is

$$\frac{\partial}{\partial x}(\rho u) + \frac{\partial}{\partial y}(\rho v) + \frac{\partial}{\partial z}(\rho w) = 0, \tag{2.8}$$

$$\frac{\partial p}{\partial x} = \frac{\partial^2 u}{\partial z^2} + O(\varepsilon Re, \varepsilon^2), \tag{2.9}$$

$$\frac{\partial p}{\partial y} = \frac{\partial^2 v}{\partial z^2} + O(\varepsilon Re, \varepsilon^2), \tag{2.10}$$

$$\frac{\partial p}{\partial z} = O(\varepsilon^3 Re, \varepsilon^2), \tag{2.11}$$

and

$$p = \rho. \tag{2.12}$$

As mentioned in the Introduction, the gas flow through a micro-channel is usually characterized by a small but non-zero Knudsen number corresponding to the slip-flow regime (Sone 2002). Consequently, the continuum model needs to be modified by imposing velocity-slip conditions on the channel walls. Thus,

$$w = 0 \quad \text{at} \quad z = \pm 1, \tag{2.13a}$$

$$(u, v) = \mp \sigma Kn \frac{\partial}{\partial z}(u, v) \quad \text{at} \quad z = \pm 1. \tag{2.13b}$$

In the conditions (2.13*b*) Kn is based on H, and σ, representing the interaction between the gas molecules and the solid wall, is related to the momentum accommodation coefficient (Maxwell 1879; Chapman & Cowling 1970). In (2.9)–(2.11) $Re = UH/\nu_{ref}$, where ν_{ref} denotes an appropriate reference value of the kinematic viscosity, is the Reynolds number. For the present limit process to be consistent it is thus necessary that εRe be asymptotically small when $\varepsilon \to 0$ (which condition is common in shallow geometrical configurations, cf. Batchelor 1967). This requirement is generally satisfied for micro-channel flows (Arkilic *et al.* 1997; Lee *et al.* 2002*a*; Yu *et al.* 2005).

Before proceeding, it is useful to consider the above assumption of isothermal conditions. Inspecting the dominant balance in (2.3), we observe that the convection, conduction, compression-work and viscous-dissipation terms are of the orders $\rho C_v (U/D)\Delta T$, $(k/H^2)\Delta T$, pU/D and $\mu(U/H)^2$, respectively. Since the Prandtl number for common gases (such as air, nitrogen etc.) is $Pr \approx 1$, the ratio of the magnitudes of convection and conduction is $\sim \varepsilon Re$ and hence the contribution of convection is negligible. Conduction balances the compression work for relative temperature differences $\Delta T/T \sim \varepsilon Re$ and the dissipation rate for $\Delta T/T \sim M^2$ where M denotes the Mach number (which is typically $\lesssim 0.1$, Lee *et al.* 2002*a,b*). We thus conclude that, when channel walls are maintained at a uniform temperature (as is often the case for micro-devices), conduction balances compression work and dissipation with negligible relative temperature variations across the fluid.
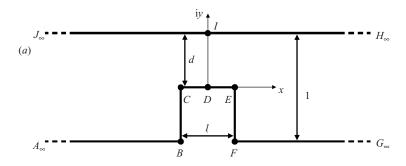
3. Analysis

Integrating (2.9) and (2.10) twice with respect to z while making use of (2.11) and (2.13*b*) we obtain for $\boldsymbol{u}_{\parallel} = (u, v)$

$$\boldsymbol{u}_{\parallel} = -\left[\tfrac{1}{2}(1 - z^2) - \sigma Kn\right] \boldsymbol{\nabla}_{\parallel} p, \tag{3.1}$$

where $\boldsymbol{\nabla}_{\parallel} = \hat{\boldsymbol{i}}\partial/\partial x + \hat{\boldsymbol{j}}\partial/\partial y$ is the planar portion of $\boldsymbol{\nabla}$. Since the mean free path is inversely proportional to the local density we may substitute $Kn = Kn_0/p$ (where Kn_0 is the value corresponding to the reference conditions) into (3.1) to obtain

$$\boldsymbol{u}_{\parallel} = -\left[\tfrac{1}{2}(1 - z^2) - \sigma \frac{Kn_0}{p}\right] \boldsymbol{\nabla}_{\parallel} p. \tag{3.2}$$

Substituting this together with (2.12) in the continuity equation (2.8) and integrating with respect to z while making use of the symmetry of the problem relative to the
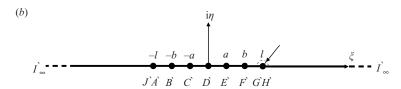
FIGURE 2. The domain of the problem in (*a*) the physical *t*-plane and (*b*) the transformed ζ-plane. ($J_\infty H_\infty$ is the symmetry line of the channel planform.)

midplane $z = 0$ yields

$$w = \frac{z}{p} \nabla_\parallel^2 \left[\tfrac{1}{4} \left(1 - \tfrac{1}{3} z^2 \right) p^2 + \sigma K n_0 p \right]. \tag{3.3}$$

From (2.13*a*) we obtain the linear equation

$$\nabla_\parallel^2 G = 0, \quad \text{defining} \quad G \triangleq \tfrac{1}{6} p^2 + \sigma K n_0 p. \tag{3.4}$$

In the absence of slip at $z = \pm 1$ (i.e. when $Kn = 0$) it immediately follows from the above that $\nabla_\parallel^2 p^2 = 0$ and thus by (3.3) w vanishes identically (Arkilic *et al.* 1997). From (3.2) we note that as is common in the lubrication approximation (Batchelor 1967) $\nabla_\parallel \times u_\parallel = 0$. Consequently, we may only impose on the sidewalls of the channel that $\hat{n} \cdot u_\parallel = 0$, where $\hat{n}$ is a unit normal perpendicular to the wall. Equivalently, by (3.1) and (3.4), $\partial G / \partial n = \hat{n} \cdot \nabla_\parallel G = 0$.

As mentioned in the Introduction, the widths of micro-channels are usually much smaller than their lengths. Subsequent analysis is thus facilitated by considering an infinite channel. Far upstream and downstream of the constriction the flow is expected to become parallel and uniform in the *y*-direction. Integrating ρu, the mass flux density, across the channel from bottom to midplane while making use of (2.12), (3.2) and (3.4) and selecting reference values at the far upstream or downstream, we obtain the far-field conditions

$$\frac{\partial G}{\partial x} = -1 \quad \text{as} \quad x \to \pm\infty. \tag{3.5}$$

To obtain $G(x, y)$ satisfying (3.2) together with the above Neumann-type boundary conditions we regard it as the real part of an analytic function $F(t) = G(x, y) + iQ(x, y)$ of the complex variable $t = x + iy$. Figure 2(*a*) presents the domain of the problem in the physical *t*-plane. (In fact, owing to the symmetry of the problem about the line $J_\infty H_\infty$, only half of the domain appears in the figure.) Let the analytic function $t = t(\zeta)$ represent a conformal mapping of the fluid domain within (half) the

micro-channel onto the upper half $\eta > 0$ of the complex $\zeta = \xi + i\eta$ plane (figure 2*b*). By the Schwarz–Christoffel theorem (Milne-Thomson 1968) and the symmetry of the problem with respect to DI, the requisite transformation is accomplished through

$$\frac{\mathrm{d}t}{\mathrm{d}\zeta} = \frac{C}{\zeta^2 - 1}\sqrt{\frac{\zeta^2 - a^2}{\zeta^2 - b^2}}. \tag{3.6}$$

The parameters C (which in general is complex) and the real $0 < a < b < 1$ are determined by specifying the geometry of the constriction through the location in the t-plane of the points I, E and F. Note that the above transformation equally applies to a channel with a cavity (instead of a constriction) when a and b are interchanged in (3.6) or, equivalently, we choose the parameters $0 < b < a < 1$. Thus, making use of the fact that $t(H_\infty) - t(G_\infty) = i$ we integrate (3.6) along a small semi-circular arc $\zeta = 1 + \delta e^{i\theta}$ ($\delta \to 0$) from $\theta = \pi$ to $\theta = 0$ (marked by the dashed line around $\zeta = 1$) to obtain

$$C = -\frac{2}{\pi}\sqrt{\frac{1 - b^2}{1 - a^2}}. \tag{3.7}$$

We could anticipate that C is real in the present problem from DE lying along the real axis of the t-plane (figure 2*a*). Selecting the branch of $(\zeta - a)^{1/2}/(\zeta - b)^{1/2}$ defined by a branch cut extending between $\zeta = a$ and $\zeta = b$ along the real axis of the ζ-plane and by being real and positive at $\zeta = 1$, (3.6) is integrated in conjunction with the condition $t(0) = 0$ to yield

$$t = -\frac{2}{\pi b}\left(\frac{1 - b^2}{1 - a^2}\right)^{1/2}\left[F\left(\frac{\zeta}{a}\bigg|\frac{a^2}{b^2}\right) - (a^2 - 1)\,\Pi\left(a^2; \frac{\zeta}{a}\bigg|\frac{a^2}{b^2}\right)\right], \tag{3.8}$$

where

$$F\left(\frac{\zeta}{a}\bigg|\frac{a^2}{b^2}\right) = \int_0^{\zeta/a}\frac{\mathrm{d}\zeta_1}{\sqrt{\left(1 - \zeta_1^2\right)\left(1 - \zeta_1^2 a^2/b^2\right)}} \tag{3.9}$$

and

$$\Pi\left(a^2, \frac{\zeta}{a}\bigg|\frac{a^2}{b^2}\right) = \int_0^{\zeta/a}\frac{\mathrm{d}\zeta_1}{\left(1 - \zeta_1^2 a^2\right)\sqrt{\left(1 - \zeta_1^2\right)\left(1 - \zeta_1^2 a^2/b^2\right)}} \tag{3.10}$$

are elliptic integrals of the first and third kinds, respectively (Abramowitz & Stegun 1964). The complex potential in the ζ-plane $F[\zeta(z)] = f(\zeta) = g + iq$ is obtained as

$$f(\zeta) = \frac{1}{\pi}\ln\frac{1 - \zeta}{1 + \zeta}. \tag{3.11}$$

Thus, for a given pair of a and b, i.e. a given channel planform, the complete solution of the problem consists of (3.11) together with (3.8). The solution $G(x, y)$ is explicitly independent of the (presumed small) value of Kn (which only appears in (3.4) relating G and the pressure).

The resulting flow may be described by means of the respective families of curves, $G = \text{const}$ (dashed) and $Q = \text{const}$ (solid) shown in figure 3. By (3.4), the former family corresponds to lines of constant pressure. Furthermore, since by definition G and Q respectively constitute the real and imaginary parts of the analytic function $F(t)$, the above families are mutually orthogonal. The lines $Q = \text{const}$ are thus tangent to $\nabla_\parallel p$. Hence, by (3.1) they constitute the streamlines of the field $\boldsymbol{u}_\parallel$ or the actual streamlines at the channel mid-plane ($z = 0$). Employing the polar representation
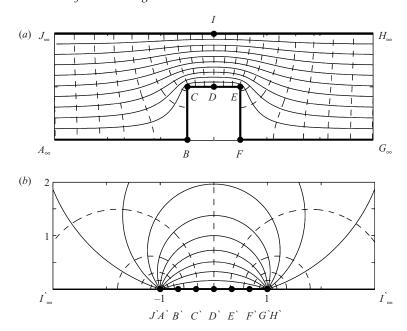
FIGURE 3. Streamlines (solid) and equi-potential lines (dashed) in (*a*) the physical *t*-plane and (*b*) the transformed ζ-plane.

$1 \mp \zeta = r_j \exp(i\theta_j)(j = 1, 2)$, (3.11) is written

$$f(\zeta) = \frac{1}{\pi} \left[\ln \frac{r_1}{r_2} + i(\theta_1 - \theta_2) \right]. \tag{3.12}$$

Thus, for $r_1/r_2 = R$, the dashed circles of radii $2cR^{1/2}/(1 - R)$ centred at $[\pm(1 + R)/(1 - R), 0]$ in figure 3(*b*) correspond to $g = $ const curves, which are the ζ-plane images of the above family $G = $ const. Furthermore, the solid circular arcs subtended by the chord $(-1, 1)$ in figure 3(*b*) mark lines of $q = $ const, the ζ-plane images of the above family $Q = $ const. (Orthogonality of both families is preserved by the conformal mapping $t = t(\zeta)$.) Figure 3(*a*) presents the flow field in the physical *t*-plane as obtained from figure 3(*b*) by use of (3.8).

We now apply the present calculation to assess the effect of the constriction on the pressure head required to drive a given mass flow rate through the micro-channel. We express the difference between the constricted channel and a uniform channel in terms of $G(x, y)$ which uniquely determines p through (3.4). The above-mentioned fore–aft symmetry of the problem governing $G(x, y)$ allows us to consider only the downstream half of the channel between $x = 0$ and $x \to \infty$. For a straight uniform channel one readily obtains that (within an arbitrary additive constant)

$$G_0 = -x \quad \text{or, equivalently,} \quad F_0 = -t. \tag{3.13}$$

From this together with the condition (3.5) it is evident that for a given mass flow rate the difference $G - G_0$ tends to a constant limit as $x \to \infty$. To obtain a measure of the pressure-head loss associated with the constriction we therefore focus on the limit

$$\Delta = \lim_{t \to \infty} \text{Re} \left\{ F(0) - F(t) - [F_0(0) - F_0(t)] \right\} = \lim_{\zeta \to 1} \text{Re} \left\{ -t(\zeta) - \frac{1}{\pi} \ln \frac{\zeta - 1}{\zeta + 1} \right\}, \tag{3.14}$$

utilizing (3.11) and (3.13). Since (cf. figure 2) $\mathrm{Re}\{t(1^-)\} = \mathrm{Re}\{t(1^+) - t(\infty)\}$, we apply (3.6) to obtain

$$\lim_{\zeta \to 1} \mathrm{Re}\left\{ t(\zeta) \right\} = \lim_{\zeta \to 1} \mathrm{Re}\left\{ \frac{2}{\pi} \left(\frac{1-b^2}{1-a^2} \right)^{1/2} \int_\zeta^\infty \left(\frac{\zeta_1^2 - a^2}{\zeta_1^2 - b^2} \right)^{1/2} \frac{\mathrm{d}\zeta_1}{\zeta_1^2 - 1} \right\}. \tag{3.15}$$

Substituting this into (3.14) and integrating by parts, the logarithmic singularities mutually cancel and we obtain

$$\Delta = \frac{1}{\pi} \left(\frac{1-b^2}{1-a^2} \right)^{1/2} \int_1^\infty \ln\left(\frac{\zeta + 1}{\zeta - 1} \right) \frac{d\zeta}{(\zeta^2 - a^2)^{1/2}(\zeta^2 - b^2)^{3/2}}. \tag{3.16}$$

From (3.14) one readily obtains that the total difference in G_0 along a finite segment of length L of the uniform channel is $\Delta G_0 = L$. Provided that L is sufficiently large so that (3.5) is already approximately satisfied at $x = \pm L/2$ (see the discussion at the beginning of §4), the corresponding difference in the constricted channel is $\Delta G = L + 2\Delta$ (the factor 2 arising from the above calculation dealing with only the respective downstream halves of both channels). Thus, 2Δ is the normalized 'equivalent length'. This term, which is in common use in the literature concerning (incompressible) viscous flows through ducts (White 1986), quantifies 'minor losses' (i.e. the additional pressure head required to compensate for the presence of bends, valves or constrictions) in terms of an additional length of a uniform straight conduit. Furthermore, the proportionality of the mass flow rate and $\partial G/\partial x$ (see the argument preceding (3.5)) together with the linearity of the problem governing $G(x, y)$ allow the calculation of the reduction due to the constriction in the mass flow rate for given entrance and exit pressures. Thus, if the mass flow rate in both (uniform and constricted) channels is equal to $\dot{m}_0$ for $\Delta G > \Delta G_0$, reducing ΔG to ΔG_0 in the constricted channel will result in a proportionally reduced rate $\dot{m}$ ($< \dot{m}_0$). From the above we thereby obtain

$$\frac{\dot{m}}{\dot{m}_0} = \frac{\Delta G_0}{\Delta G} = \left(1 + \frac{2}{L}\Delta \right)^{-1}. \tag{3.17}$$

We emphasize that Δ depends only upon the geometrical parameters of the constriction and upon neither the entrance or exit conditions (Kn, pressures, etc.) nor the specific properties of the gas (provided, of course, that it satisfies the equation of state (2.4)). It thus seems desirable to express Δ explicitly in terms of l and d, the geometric parameters characterizing the constriction (figure 2), rather than in terms of a and b, the parameters of the transformation (3.6). This calculation is outlined in the Appendix and the results are presented in the next section.

4. Results and discussion

The analysis of the preceding section is based on the assumptions that ε and εRe are both asymptotically small. To examine the resulting approximation we have numerically simulated (by means of the finite element COMSOL 3.3 software package) the flow of air through 1 µm-deep shallow constricted channels for diminishing values of ε and εRe. Unlike the analytic approximation, the simulated fluid motion is governed by the complete set of the three-dimensional continuity, Navier–Stokes and energy equations for a perfect Newtonian gas. A uniform temperature (293 K) is prescribed at the channel walls and uniform pressures and temperatures are assumed at the entrance and exit cross-sections, respectively. The exit pressure is atmospheric
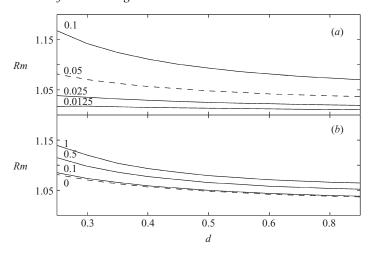
FIGURE 4. Variation with d, the dimensionless gap (see figure 1), of the ratio Rm between the mass flow rates obtained from the analytic approximation and the numerical simulation, respectively, for (a) $Re = 0$ and the indicated values of ε; (b) $\varepsilon = 0.05$ and the indicated values of εRe. In all cases the normalized length of the constriction is $l = 0.5$. For comparison the case $\varepsilon = 0.05$ and $Re = 0$ (marked by the dashed lines) appears in both parts.

and the entry pressure is adjusted so as the achieve the requisite values of Re. To simplify the comparison no-slip conditions at the walls are imposed in the simulations. The corresponding analytic solution is accordingly calculated by substituting $Kn_0 = 0$ in the relation (3.4) between p and G, thus ensuring that (as far as possible within the limitations of the lubrication approximation) the analytic solution employed in the comparison also satisfies the no-slip conditions.

We have selected for our COMSOL simulations a tetrahedral unstructured mesh. In general, variations of the various fields in the x- and y-directions are expected to be slower than in the z-direction. Nevertheless, to avoid convergence problems, cell dimensions in all directions need to be of comparable lengths. This, together with the division of the distance between the channel bottom and its midplane into at least four cells, places a lower bound on the total number of cells for a given channel configuration, imposing computational limitations on the smallest value of ε and the largest total length of the simulated domain which are practically realizable. The latter parameter is selected so that a uniform fully developed flow is established across the channel width at both the entrance and exit sections. An initial estimate of the required length is based on the analytic solution and is later refined according to the numerical results. In general, the length (which is sufficient to ensure that the variance of G across both the entrance and exit sections of the simulation domain be smaller than $\approx 10^{-6}$) is essentially determined by the constriction gap width. The results indicate that, for all $d \geqslant 1/4$, this (dimensionless) length is smaller than ≈ 2.5 both upstream and downstream of the constriction. To avoid excessive computational effort we have thus performed these simulations only for $d \geqslant 1/4$.

A global measure of the difference between numerical and analytic calculations is provided by Rm, the ratio between the respective analytically and numerically obtained mass flow rates. The analytic calculation (3.17) consists of two elements: calculation of $\dot{m}_0$ through the corresponding uniform channel and the effect of the constriction embodied in Δ (3.16). The latter only depends upon the geometrical parameters; in accordance with the above, $\dot{m}_0$ is calculated for $Kn_0 = 0$. Figure 4 thus presents the variation of Rm with d for $l = 1/2$ and the indicated values of ε
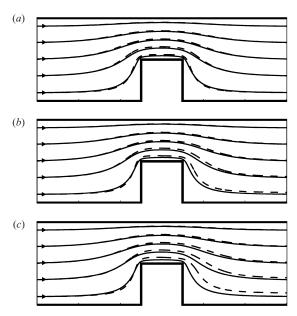
FIGURE 5. Streamline patterns at the mid-plane of a constricted channel ($l, d = 0.5$) as obtained from the analysis (solid) and numerical simulation ($\varepsilon = 0.05$, dashed) for (*a*) $Re = 0$, (*b*) $Re = 10$ and (*c*) $Re = 20$.

(*a*) and εRe (*b*). To isolate the respective impacts of diminishing ε and diminishing inertial effects we take $Re = 0$ in part (*a*) of the figure. We observe that for each curve Rm is increasing with decreasing d. This reflects the fact that with diminishing constriction gap width the 'local' value of ε is effectively increasing. We further observe that Rm is approaching unity nearly linearly with decreasing ε, whereas for $Re = 0$ the error in (2.9)–(2.12) is $O(\varepsilon^2)$. This $O(\varepsilon)$ error results from the failure of $\boldsymbol{u}_\parallel$ to satisfy the no-slip boundary condition on the channel sidewalls (which is inherent in the lubrication approximation, see the discussion of the boundary conditions following (3.4)). Figure 4(*b*) describes for $\varepsilon = 0.05$ and diminishing values of εRe the convergence of Rm to the corresponding curve from Figure 4(*a*) (which is here marked by the dashed line). When $\varepsilon Re \lesssim 0.1$ ($Re \lesssim 2$) the curves are nearly indistinguishable.

Figure 5 compares the streamline patterns in the mid-plane of the flow (from left to right) through a constricted channel ($l, d = 1/2$) as obtained from the analytic solution (3.8) and (3.11) (solid lines) and from the numerical simulations (dashed lines) for $\varepsilon = 0.05$ and the finite values of $Re = 0$ (*a*), 10 (*b*) and 20 (*c*) (corresponding to three of the curves presented in figure 4(*b*)). The analytically obtained streamline pattern possesses fore–aft symmetry. The same is true of the numerically simulated pattern at $Re = 0$. The relatively small differences between both patterns in part (*a*) are related to the finite value of ε ($= 0.05$) in the numerical simulation. With increasing Re in parts (*b*) and (*c*), the simulated patterns become increasingly asymmetric demonstrating the rapidly growing inaccuracy of the analytic solution for $Re \gtrsim 10$ (which is not surprising considering that $\varepsilon Re \gtrsim 0.5$ no longer qualifies as asymptotically small). While no flow reversal has been detected in our simulations up to $Re = 20$, the numerically computed (dashed) pattern in Figure 5(*c*) indicates an impending flow separation from the lee-side of the constriction. Evidently, the present analysis which is based on the lubrication approximation cannot predict this.
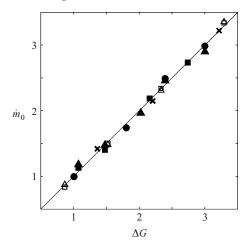
FIGURE 6. Experimental data for normalized mass flow rates $\dot{m}_0$ and the corresponding values of ΔG for the flow through symmetrically constricted micro-channels (Lee *et al.* 2002*b*) of total length 4000 μm, width 40 μm and depth 1 μm ($\varepsilon = 0.025$), dimensionless constriction length $l = 0.5$ and gap width $d = 0.85$ (■), 0.7 (▲), 0.5 (●) and 0.25 (×). Also presented are measurements in micro-channels with symmetric multiple cavities (Yu *et al.* 2005). The total length of these channels is 3825 μm, their width 30 μm and depth 1.7 μm ($\varepsilon = 0.057$), the dimensionless length of the cavities is $l = 1$, their gap width is $d = 2$ and their total numbers are 63 (□) and 127 (△).

The onset of flow separation in micro-channel configurations (e.g. cavities, sudden expansions, etc.) has been studied by Yu *et al.* (2005) and Tsai *et al.* (2007) by means of flow visualizations and simulations. Their measurements and numerical results are correlated by flow-regime maps in the plane of *Re* and a geometric parameter (related to ε) indicating that small-*Re* separation is only possible for ε exceeding a certain threshold value (≈ 0.15 when relating the geometric parameter of Yu *et al.* 2005, to ε through the smallest dimension of the present planform). In terms of the present parameters, the results of Yu *et al.* (2005) predict that for $\varepsilon = 0.05$ flow separation only appears at $Re \gtrsim 25$ (which is in agreement with our above comments regarding the simulated streamline pattern in figure 5(*c*)). These observations indicate that the flow is indeed fully attached for sufficiently small finite values of ε and εRe.

As mentioned above, the mass flux density along the micro-channel is proportional to $\partial G/\partial x$ and G is governed by a linear problem (which are fundamental attributes of the lubrication approximation applied to the shallow micro-channel). Consequently, the mass flow rate is linear in ΔG, the total difference between the values of G at the entrance and exit sections, respectively. Figure 6 presents a compilation of experimental results reported by Lee *et al.* (2002*b*) and Yu *et al.* (2005) regarding the mass flow rate in constricted and multi-cavity micro-channels, respectively. The values of ΔG are calculated by substituting the reported Knudsen numbers and entrance pressures (the exit pressures are atmospheric) in the definition (3.4). They are plotted versus the mass flow rates in the figure. (For each configuration the reported mass flow rates are calibrated by a constant multiplication factor so as to make the proportionality coefficient with ΔG equal to unity.) The linear correlation evident in the figure (which is typical of low-Mach-number viscous compressible flows in uniform long micro-channels, Beskok *et al.* 1996) supports our use of the lubrication approximation in the present analysis, indicating that the effect of flow separation (if any) in these micro-channels is rather small.
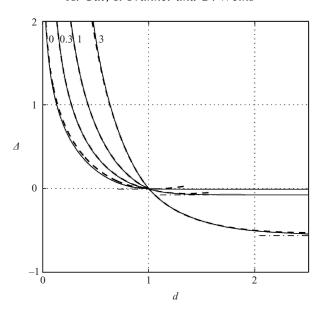
FIGURE 7. The effect of l (values indicated), the constriction (cavity) length, on the variation of Δ with d, the gap width. Solid lines are obtained for $l \neq 0$ via numerical quadratures of (3.16), (A1) and (A2) and for $l = 0$ from (4.1). Dashed and dashed-dotted lines represent (4.2) and (4.3), respectively.

We next examine the effect of the geometrical configuration on Δ representing the pressure-head or mass-flow-rate losses. Figure 7 thus describes the variation of Δ with the gap width for both constrictions ($0 < d < 1$) and cavities ($d > 1$) at the indicated values of the dimensionless length l. The solid lines mark exact calculations of $\Delta(a, b)$, $d(a, b)$ and $l(a, b)$ via numerical quadratures of (3.16), (A1) and (A2), respectively. An exception is $l = 0$ for $0 < d < 1$ corresponding to $a = 0$ (see (A3) and figure 2). For this case we obtain the closed-form expression

$$\Delta_0 = -\frac{2}{\pi} \ln \left[\sin \left(\frac{2}{\pi} d \right) \right]. \tag{4.1}$$

The dashed lines represent the approximation

$$\Delta \sim \frac{1}{2} \frac{1-d}{d} l + \frac{1}{\pi} \left[2 \ln \left| \frac{1-d^2}{4d} \right| + \frac{1+d^2}{d} \ln \left| \frac{1+d}{1-d} \right| \right], \tag{4.2}$$

obtained in the Appendix and the horizontal dash-dotted asymptotes represent the limit of deep cavities ($d \to \infty$) when (see the Appendix)

$$\Delta = \frac{1}{\pi} \ln \left(\frac{l^2+4}{4} \right) - l \left\{ \frac{1}{2} - \frac{1}{\pi} \cos^{-1} \left[\frac{l}{(l^2+4)^{1/2}} \right] \right\}. \tag{4.3}$$

All the curves descend monotonically with d passing through $\Delta = 0$ at $d = 1$ (i.e. a uniform channel). The variations of Δ are larger for a constriction, increasing indefinitely with diminishing gap, than for a cavity where increasing the depth cannot reduce Δ below the limit (4.3). Thus, for all $l \leqslant 0.3$ and $d > 1$, Δ is vanishingly small. Evidently, the respective effects for both constrictions and cavities become more substantial with increasing length.

With the exception of $l = 0$, the approximation (4.2) is remarkably accurate throughout the range of constrictions. In fact, even for l as small as ≈ 0.1 (not presented in the figure), the dashed and solid lines are already nearly indistinguishable from each other. Furthermore, as is clearly visible for $l = 3$, when (with increasing $d > 1$) the dashed curve starts to deviate from the solid line the latter is already close to the dash-dotted asymptote (4.3). Evidently, the explicit expression of Δ in terms of l and d is most useful, allowing a simple interpretation of the effects of the geometrical configuration on Δ. Thus, the first term, which is linear in l, represents the increase (for $d < 1$) or reduction (for $d > 1$) of the hydrodynamic resistance per unit length of an infinite straight channel resulting from changing its uniform width from unity to d. The rest of the expression on the right-hand side of (4.2), which is independent of l, represents 'end effects' associated with the transitions between the uniform channel and the constriction (or cavity) zone. Comparison of the solid and dashed curves in figure 7 demonstrates that this approximate description of end effects is not very different from the exact result (4.1) for a constriction of zero length $l = 0$.

The approximation (4.2) has been obtained in the Appendix as a leading-order asymptotic estimate in the limit $a, b \to 1$. As such, the above-observed accuracy of (4.2) seems rather surprising. Inspection of (A1) and (A2) reveals that throughout much of the domain of the parameters l and d (particulary for $d < 1$), a and b are both close to unity. *A posteriori* (4.2) turns out to be accurate provided that neither a nor b are much smaller than 1 (i.e. a small constriction length or a deep cavity, respectively). As mentioned above, in these limits Δ is closely approximated by (4.1) or (4.3) respectively.

The results of the present analysis are in agreement with those of Yu *et al.* (2005) as opposed to earlier results from the same group (Lee *et al.* 2002*b*). There is an apparent difficulty in the application of results obtained from the above analysis strictly pertaining to a single constriction or cavity within an infinitely long channel to the present multi-cavity problem. However, Yu *et al.* (2005) observe that when the distance between adjacent cavities exceeds the length of a single cavity, the total effect is linear in the number of cavities. This suggests that the effects of multiple cavities are additive thereby demonstrating that hydrodynamic interactions between the various cavities along the channel are negligible. This view is also supported by the present analytic solution which shows that halfway between the adjacent cavities the flow field restores uniformity (in the y-direction) across the channel. We can thus estimate the effect of the multiple cavities on the mass flow rate by making use of (3.17) for a 'unit cell' whose length L is the sum of the cavity length and the distance between adjacent cavities. Consider the multi-cavity micro-channels of Yu *et al.* (2005) whose total length, width and depth are 3825 μm, 30 μm and 1.7 μm, respectively. The length and width of each cavity as well as the distance between the adjacent cavities are all equal to 15 μm. In terms of the parameters of the present analysis $l = 1$, $d = 2$ and $L = 2$. For these values (see figure 7) Δ already coincides with the asymptote (4.3) which readily yields $\Delta \approx -0.076$. From (3.17) we then obtain that the corresponding mass flow rate increases by $\approx 8\%$ relative to a uniform channel whereas Yu *et al.* (2005) estimate the average increase as $\approx 7\%$. Considering the approximations involved (e.g. $\varepsilon \approx 0.057$ in the actual channel while our analysis strictly applies when $\varepsilon \to 0$) the agreement is satisfactory.

Equation (3.17) together with (4.2) provide a useful approximation allowing a straightforward estimate of the effect of the constriction for practically any combination of the geometrical parameters. Furthermore, the present scheme is in

principle applicable to any shallow micro-configuration whose planform qualifies as a generalized polygon (cf. Milne-Thomson 1968). Considering the current fabrication technology (e.g. of silicon micro-devices) this requirement is met in a wide variety of micro-fluidics problems.

Appendix Approximate explicit expressions for $\Delta(l, d)$

By (3.8) and figure 2

$$d = 1 - \frac{2}{\pi} \left(\frac{1 - b^2}{1 - a^2} \right)^{1/2} \int_a^b \left(\frac{\xi^2 - a^2}{\xi^2 - b^2} \right)^{1/2} \frac{\mathrm{d}\xi}{1 - \xi^2} \tag{A1}$$

and

$$l = \frac{4}{\pi} \left(\frac{1 - b^2}{1 - a^2} \right)^{1/2} \int_0^a \left(\frac{a^2 - \xi^2}{b^2 - \xi^2} \right)^{1/2} \frac{\mathrm{d}\xi}{1 - \xi^2}. \tag{A2}$$

Furthermore, making use of (3.14) and (3.15) we obtain the alternative expression

$$\Delta = \frac{2}{\pi} \int_1^\infty \left[1 - \left(\frac{\xi^2 - a^2}{\xi^2 - b^2} \right)^{1/2} \left(\frac{1 - b^2}{1 - a^2} \right)^{1/2} \right] \frac{\mathrm{d}\xi}{1 - \xi^2}. \tag{A3}$$

4.1. *The limit $a, b \to 1$*

Defining the parameters $0 < \beta \leqslant \alpha \ll 1$ through

$$a = 1 - \alpha, \quad b = 1 - \beta \tag{A4}$$

and replacing ξ, the integration variable in (A1) and (A2), by $\xi_1 = 1 - \xi$, we obtain to leading order in (α, β)

$$d \sim 1 - \frac{1}{\pi} \left(\frac{\beta}{\alpha} \right)^{1/2} \int_\beta^\alpha \left(\frac{\alpha - \xi_1}{\xi_1 - \beta} \right)^{1/2} \frac{\mathrm{d}\xi_1}{\xi_1} \sim \left(\frac{\beta}{\alpha} \right)^{1/2}. \tag{A5}$$

Similarly, from (A2)

$$l \sim \frac{4}{\pi} \left(\frac{\beta}{\alpha} \right)^{1/2} \int_\alpha^1 \left(\frac{2\xi_1 - \xi_1^2 - 2\alpha}{2\xi_1 - \xi_1^2 - 2\beta} \right)^{1/2} \frac{\mathrm{d}\xi_1}{\xi_1 (2 - \xi_1)}. \tag{A6}$$

To estimate l we divide the interval $(\alpha, 1)$ into the sub-intervals (α, γ) and $(\gamma, 1)$ where $\alpha \ll \gamma \ll 1$. Making use of the approximations respectively appropriate to each of the sub-intervals we obtain

$$l \sim \frac{2}{\pi} \left(\frac{\beta}{\alpha} \right)^{1/2} \left[\int_\alpha^\gamma \left(\frac{\xi_1 - \alpha}{\xi_1 - \beta} \right)^{1/2} \frac{\mathrm{d}\xi_1}{\xi_1} + 2 \int_\gamma^1 \frac{\mathrm{d}\xi_1}{(2 - \xi_1)\xi_1} \right]$$

$$\sim \frac{2}{\pi} \left[\left(\frac{\beta}{\alpha} \right)^{1/2} \ln \left(\frac{8}{\alpha - \beta} \right) - \ln \left(\frac{\alpha^{1/2} + \beta^{1/2}}{\alpha^{1/2} - \beta^{1/2}} \right) \right]. \tag{A7}$$

To obtain an approximate expression for Δ we change the integration variable in (A3) to $\xi_2 = 1 - \xi$. The interval of integration $(0, \infty)$ is then separated into the sub-intervals $(0, \gamma)$ and (γ, ∞), respectively. Utilizing the approximations respectively valid in each of the sub-intervals we eventually obtain

$$\Delta \sim \frac{1}{\pi} \left\{ \ln \left[\frac{1}{2} \left(\frac{\alpha^{1/2} + \beta^{1/2}}{\alpha^{1/2} \beta^{1/2}} \right)^2 \right] + \left(\frac{\beta}{\alpha} \right)^{1/2} \ln \left[\frac{(\alpha^{1/2} + \beta^2)^{1/2}}{8} \right] \right\}. \tag{A8}$$

The ratio β/α is available from (A5). Making use of this and (A7) to express $\ln \alpha$ in terms of l and d and substituting in (A3) we readily obtain $\Delta(l, d)$ for $0 < d \leqslant 1$. When $1 < d$ (a cavity) we need to consider the limit $0 < \alpha \leqslant \beta \ll 1$. The only difference from the above calculation is that in (A7) the arguments of the logarithmic terms are now replaced by their respective absolute values. The same applies to $\Delta(l, d)$ as appears in (4.2) for all $0 < d < \infty$.

4.2. *The limit $b \to 0$ (a deep cavity)*

For $d > 1$ the parameters a and b are interchanged in the integration limits in (A1) and (A2). When $b \to 0$ with a fixed we obtain from (A2)

$$l \sim \frac{4a}{\pi} \left(1 - a^2\right)^{1/2} \int_0^b \left(b^2 - \zeta^2\right)^{-1/2} \mathrm{d}\zeta = \frac{2a}{\left(1 - a^2\right)^{1/2}}. \tag{A9}$$

For the gap width we separate the integration interval (b, a) into the sub-intervals (b, γ) and (γ, α) where $b \ll \gamma \ll a$ and obtain to leading order

$$d \sim 1 - \frac{2}{\pi} \left[\frac{a}{\left(1 - a^2\right)^{1/2}} \ln \left(\frac{b}{4a}\right) - \sin^{-1} a \right], \tag{A10}$$

verifying that d indeed diverges in this limit. For Δ we obtain from (A3)

$$\Delta \sim -\frac{1}{\pi} \left[\frac{2a}{\left(1 - a^2\right)^{1/2}} \left(\frac{\pi}{2} - \cos^{-1} a\right) + \ln \left(1 - a^2\right) \right]. \tag{A11}$$

Expressing a in terms of l by means of (A9) we readily obtain (4.3) from (A11).

REFERENCES

ABRAMOWITZ, M. & STEGUN, I. A. 1964 *Handbook of Mathematical Functions*. Dover.
ARKILIC, E. B., SCHMIDT, M. A. & BREUER, K. S. 1997 Gaseous slip flow in long microchannels. *J. Microelectromech. Syst.* **6**, 167–178.
BATCHELOR, G. K. 1967 *An Introduction to Fluid Dynamics*. Cambridge University Press.
VAN DEN BERG, H. R., TEN SELDAM, C. A. & VAN DER GULIK, P. S. 1993 Compressible laminar flow in a capillary. *J. Fluid Mech.* **246**, 1–20.
BESKOK, A., KARNIADAKIS, G. E. & TRIMMER, W. 1996 Rarefaction and compressibility effects in gas microflows. *Trans. ASME: J. Fluids Engng* **118**, 448–456.
CERCIGNANI, C. 2000 *Rarefied Gas Dynamics*. Macmillan.
CHAPMAN, S. & COWLING, T. G. 1970 *The Mathematical Theory of Non-uniform Gases*. Cambridge University Press.
FAN, Q., XUE, H. & SHU, C. 1999 DSMC simulations of gaseous flows in microchannels. In *5th ASME/JSME Joint Thermal Engineering Conference March 15-19 1999, San Diego, California*.
GAD-EL-HAK, M. 1999 The fluid mechanics of microdevices. *Trans. ASME: J. Fluids Engng* **121**, 5–33.
GRAUR, I. A., MEOLANS, J. G. & ZEITOUN, D. E. 2005 Analytical and numerical description for isothermal gas flow in microchannels. *Microfluid Nanofluid* **2**, 64–77.
HARLEY, J. C., HUANG, Y., BAU, H. H. & ZEMEL, J. N. 1995 Gas flow in micro-channels. *J. Fluid Mech* **284**, 257–274.
HO, C. M. & TAI, Y. C. 1996 Mems and its applications for flow control. *Trans. ASME: J. Fluids Engng* **118**, 437–447.
HO, C. M. & TAI, Y. C. 1998 Micro-electro-mechanical-systems (MEMS) and fluid flows. *Annu. Rev. Fluid Mech.* **30**, 579–612.
LEE, W. Y., WONG, M. & ZOHAR, Y. 2001 Gas flow in microchannels with bends. *J. Micromech. Microengng* **11**, 635–644.

LEE, W. Y., WONG, M. & ZOHAR, Y. 2002*a* Microchannels in series connected via a contraction/expansion section. *J. Fluid Mech* **459**, 187–206.

LEE, W. Y., WONG, M. & ZOHAR, Y. 2002*b* Pressure loss in constriction microchannels. *J. Microelectromech. Syst* **11**, 236–244.

LIU, J. Q., TAI, Y. C. & HO, C. M. 1995 MEMS for pressure distribution studies of gaseous flows in microchannels. In *Proc. IEEE Micro-electromech. Syst*, pp. 209–215.

MAXWELL, J. C. 1879 On stresses in rarified gases arising from inequalities of temperature. *Phil. Trans. R. Soc. Lond.* **170**.

MILNE-THOMSON, L. M. 1968 *Theoretical Hydrodynamics*. Macmillan.

PONG, K., HO, C. & TAI, Y. 1994 Non-linear pressure distribution in uniform microchannels. ASME-FED vol. 197, pp. 51–56.

PRUD'HOMME, R., CHAPMAN, T. & BOWEN, J. 1986 Laminar compressible flow in a tube. *Appl. Sci. Res.* **43**, 67–74.

QIN, F.-H., SUN, D.-J. & YIN, X.-Y. 2007 Perturbation analysis on gas flow in a straight microchannel. *Phys. Fluids* **19**.

SHARIPOV, F. 1999 Non-isothermal gas flow through rectangular microchannels. *J. Micromech. Microengng* **9**, 394–401.

SONE, Y. 2002 *Kinetic Theory and Fluid Dynamics*. Birkhauser.

TSAI, C.-H., CHEN, H.-T., WANG, Y.-N., LIN, C.-H. & FU, L.-M. 2007 Capabilities and limitations of 2-dimensional and 3-dimensional numerical methods in modeling the fluid flow in sundden exapansion microchannels. *Microfluid Nanofluid* **3**, 13–18.

WHITE, F. M. 1986 *Fluid Mechanics,* 2nd edn. McGraw-Hill.

YAO, Z.-H., HE, F., DING, Y.-T., SHEN, M.-Y & WANG, X.-F. 2004 Low-speed gas flow subshocking phenomenon in a long-constant-area microchannel. *AIAA J.* **42**, 1517–1521.

YU, Z. T. F., LEE, Y.-K., WONG, M. & ZOHAR, Y. 2005 Fluid flows in microchannels with cavities. *J. Microelectromech. Syst.* **14**, 1386–1398.

ZOHAR, Y., LEE, S. Y. K., LEE, W. Y., JIANG, L. & TONG, P. 2002 Subsonic gas flow in a straight and uniform microchannel. *J. Fluid Mech.* **472**, 125–151.